Check for updates

Influence of oxidation on the magnetism of small Co oxide clusters probed by Stern–Gerlach deflection†

Kobe De Knijf ✦ *[a] Johan van der Tol,[a] Piero Ferrari, ✦ [a] Sandrien Scholiers,[a] Gao-Lei Hou ✦ [b] Peter Lievens ✦ [a] and Ewald Janssens ✦ *[a]

We report on the magnetic properties of small neutral suboxide Co_nO_m (n = 5–18 and m = 0–10, $m \leq n$) clusters produced by laser vaporisation and gas aggregation. Their magnetism is probed experimentally by means of Stern–Gerlach magnetic deflection. The results imply that the cobalt atoms couple ferromagnetically not only in pure Co_n clusters, as known from previous investigations, but also in their oxidized counterparts. It was found that the magnetic moment per cobalt atom is mostly enhanced in the oxide clusters with respect to the pure cobalt clusters and generally increases with the oxygen content in the studied composition range. The spin magnetism of selected clusters is also investigated by density functional theory (DFT) calculations. The computations allow to attribute the effect of oxidation on the magnetic response of the Co_nO_m clusters to electron transfer from the cobalt 3d and 4s valence orbitals to oxygen. The cobalt 3d levels preferentially donate electrons of minority spin, but both spin orientations are involved in the transfer of cobalt 4s electrons.

1 Introduction

Transition metal oxides play an important role in a vast variety of valuable applications.[1–4] In particular, Co oxides can be used as catalysts,[4,5] gas sensors,[6] and in the development of magnetic recording media.[7] Moreover, Co oxide nanoparticles are candidates to inhibit cancer cell growth[8,9] and have great potential as antimicrobial agents.[2,8] More specifically, there is a lot of interest in magnetic nanoparticles because they are promising candidates for diverse applications such as drug delivery, tissue engineering, biosensing, magnetic resonance imaging, ultrahigh density data storage, and magneto-electric memory devices.[10] Also, clusters with interesting properties could potentially be assembled into larger nanostructured materials.[11] Furthermore, in the interest of developing fundamental understanding of the evolution of magnetism with size

and composition from single atoms to the bulk, small clusters are ideal test systems.

It is well known that the physical and chemical properties of few-atom clusters can be distinctively different from those of their bulk counterparts with possibly even drastic differences between successive sizes.[12,13] This is also the case for cobalt oxide clusters which have been the subject of several theoretical and experimental studies examining various properties. Experimentally, efforts were undertaken to investigate them by means of photofragmentation,[14,15] photoelectron spectroscopy,[16] and infrared vibrational spectroscopy.[17] Also the role of cobalt oxide clusters as catalysts[18] and their reaction with different gases[19] have been studied. However, the magnetism of these clusters in the size range of this work has not yet been probed experimentally. In contrast, several theoretical studies explored the magnetism of cobalt oxide clusters.

A systematic DFT computational study on the magnetic properties of neutral and cationic $Co_nO_m^{0,+}$ clusters (n = 3–8, m = 1–10) was carried out by Aguilera-del-Toro and coworkers.[20] In line with multiphoton dissociation experiments, their calculations for the charged species confirmed n = m as the favoured stoichiometry, the loss of O_2 as the preferred fragmentation channel, and the particular high stability of $Co_4O_4^+$. For the latter cluster they found indications that the local spin magnetic moments at the Co sites closely resemble those of metallic Co_4 and Co_4^+, with additional significant contributions of the oxygen atoms to the total spin magnetic moment. Because of

[a] *Quantum Solid-State Physics, Department of Physics and Astronomy, KU Leuven, Celestijnenlaan 200D, 3001 Leuven, Belgium. E-mail: kobe.deknijf@kuleuven.be, ewald.janssens@kuleuven.be*

[b] *MOE Key Laboratory for Non-Equilibrium Synthesis and Modulation of Condensed Matter, School of Physics, Xian Jiaotong University, Xi'an, 710049, P. R. China*

† Electronic supplementary information (ESI) available: A schematic overview of the experimental setup, a brief explaination about the determination of the magnetic field, results from the DFT calculations on selected $Co_{6,7}O_m$ clusters (including the density of states of Co_6O_m, partial electron charges, Wiberg bond indices, and natural electron configurations), and beam profiles of all identified Co_nO_m clusters. See DOI: https://doi.org/10.1039/d2cp05202d

the parallel coupling of all local spin magnetic moments in $Co_4O_4^+$, its total spin magnetic moment is about 30% larger than that of the Co_4^+ cation. More generally, their DFT calculations predict the series of $(CoO)_n^+$ ($n = 2$–6) clusters to be stabilized by a high spin magnetic moment and that the spin-polarisation of the Co atoms is not quenched by the oxygen. The high stability of the $Co_4O_4^+$ cation was suggested by Tung *et al.*[21] as well, and photodissociation mass spectrometry also indicated that $Co_2O_2^+$ and $Co_4O_3^+$ could be particularly stable. In addition, Zayed *et al.*[22] reported the remarkable structural stability of $Co_4O_4^{0,+}$ determined by mass spectrometry, and confirmed by DFT computations for the neutral counterpart.

In another study, Gutsev *et al.* performed DFT calculations on the geometries, total spin magnetic moments, polarizabilities and binding energies of neutral $(FeO)_n$, $(CoO)_n$, and $(NiO)_n$ clusters for $n = 1$–10. In all cases, they found relatively low spin multiplicities.[23] In contrast to the neutral cobalt oxides in ref. 20 with non-vanishing total spin magnetic moments, it was concluded that the total spin magnetic moments of the bare neutral Fe_n and Co_n clusters are strongly reduced in their corresponding oxides. Ferromagnetic ordering was only found in the nickel oxides $(NiO)_n$ for $n = 3$, 4, 9, and 10, whereas $(FeO)_2$, $(CoO)_2$, $(FeO)_4$, $(CoO)_4$, $(FeO)_6$, $(CoO)_6$, and $(NiO)_5$ were found to be antiferromagnetic singlets. All other clusters in the $(FeO)_n$ and $(CoO)_n$ series as well as $(NiO)_7$ and $(NiO)_8$ were identified as being ferrimagnetic.

Recently, Geng *et al.* reported on a special class of neutral oxygen-passivated metal oxides with a cubic structure and special aromatic stability, termed 'metalloxocubes', for which enhanced stabilities of $M_{13}O_8^{0,\pm}$ (M = Fe, Co or Ni) clusters were observed.[24] In particular, the $Co_{13}O_8$ cluster has a prominent abundance in the resultant mass spectrum when neutral cobalt clusters, produced by a laser evaporation source, were allowed to interact with He gas enriched with a large oxygen content. First-principles calculations attributed the stability of this cluster to a perovskite-like body-centered cubic structure and cubic aromaticity from multicenter Co–Co metal–metal bonding. Their computations predict $Co_{13}O_8$ to have a large total spin magnetic moment of about 30 μ_B in its lowest energy state.

In the following, we present the results obtained by Stern–Gerlach magnetic deflection as well as DFT analysis on the magnetic properties of small Co_nO_m ($n = 5$–18, $m = 0$–10) clusters. We start with a description of the methodology and of the applied models to determine the experimental magnetic moments. Because of the importance of the cluster temperature in these models, attention is devoted to asses this temperature before examining the magnetism. Finally, the ferromagnetic coupling between the cobalt atoms and the influence of electron transfer from cobalt to oxygen on the magnetism is discussed.

2 Methodology

2.1 Experimental methodology

A schematic overview of the experimental setup, in more detail described in ref. 25, is provided in the ESI† (see Fig. S1).

We used a pulsed (10 Hz) laser ablation source to produce a molecular beam of clusters. The source body is a copper block that has a 3 mm diameter formation channel. The second harmonic (532 nm) of a pulsed Nd-YAG laser (Continuum Minilite II) is directed onto a translating rectangular cobalt target. The resulting evaporated material nucleates and grows into clusters in the formation channel by collisions with the atoms of a carrier gas, introduced by a pulsed supersonic valve (Jordan TOF Products, Inc.) at a backing pressure of 5 bar. A mixture of He and a small amount of oxygen (*ca.* 0.06 mol%) was used as the carrier gas, leading to the formation of cobalt suboxides, including some pure cobalt clusters. A cryogenic system, consisting of a cold head (Leybold COOLPOWER 10 MD) pneumatically driven by a closed helium circuit from a compressor unit (Leybold COOLPAK 6000 H), provides for the cooling of the source. Hereto, a conducting copper braid serves as the connection between the source and the cold head. The temperature of the formation channel was estimated to be 49 ± 2 K by a sensor on the outside of the source body. However, the actual temperature of the clusters inside the source is more reliably determined from a velocity distribution analysis,[26] as will be elaborated further, and was found to be slightly lower: 41 ± 4 K.

During their time spent in the source, the clusters are carried towards the nozzle of the formation channel, after which they expand in vacuum. The direction of the molecular beam exiting the source is denoted by x. More downstream, a skimmer removes most of the carrier gas, and the combination of a rotating chopper wheel and pulsed postionisation later in the setup selects clusters within a very narrow velocity range: here 537 ± 4 m s^{-1}, around the mean value (525.9 ± 0.1 m s^{-1}) of the average velocities of all cluster sizes in this study. A highly directional molecular beam for the magnetic deflection experiment is further achieved by means of two slit collimators, each with an opening of 0.45 mm. The collimated beam is then steered through a 2.6 mm opening between the 20 cm long poles of a Rabi type magnet, ensuring a fairly constant magnetic field gradient (about 350 T m^{-1}) along the cluster path. Neutral clusters can be deflected from their straight path by the magnet and the degree of deflection depends on the projection of their magnetic moment along the magnetic field direction. The direction of deflection is denoted by z and is orthogonal to x. About 80 cm after exiting the magnet, the clusters are subject to the aforementioned postionisation by the UV light (157 nm) of an F_2 excimer laser (Coherent ExciStar XS). The profile of this excimer laser is elongated along the deflection direction by a cylindrical lens to ensure that deflected clusters are ionized as well, and to prevent multiple photon absorption and fragmentation. The specific laser profile is estimated from a series of atomic yttrium deflection experiments, and is found to be non-uniform. The resulting profile is taken into account to assess the position dependent ionisation efficiency and to reconstruct the deflection profiles of the clusters. Once ionized, the charged clusters are extracted in the y direction, orthogonally to the x–z plane (see ESI,† Fig. S1), into a reflectron time-of-flight mass spectrometer with a

172 | *Phys. Chem. Chem. Phys.*, 2023, **25**, 171–182

This journal is © the Owner Societies 2023

position sensitive microchannel plate delay line detector (surface concept GmbH) that is able to record simultaneously the position and arrival time of each cluster.

2.2 Computational methodology

DFT calculations on selected cobalt oxide clusters, Co_6O_m ($m = 0, 4, 5, 6$) and Co_7O_m ($m = 0, 3, 4, 5$), were conducted using the ORCA 5.0 software package.[27] The hybrid PBE0 functional[28] was employed, in conjunction with the def2-TZVP basis set.[29] Tight convergency criteria were used for the self-consistent field[27] and geometry optimisation cycles. The structures of neutral cobalt clusters, Co_n, were investigated earlier by a combination of IR-UV two-colour vibrational spectroscopy and DFT calculations.[30] The geometries of Co_6 and Co_7 were taken from this work and reoptimized at the PBE0/def2-TZVP level for different multiplicities. Initial geometries of the cobalt oxide clusters were taken from the computational work of ref. 20 and reoptimized at the same level of theory. Additional possible structural isomers were generated from scratch by randomly positioning the different atoms and geometry optimisation, but no configurations of lower energy were found than the ones in ref. 20. In all cases, different spin multiplicities were considered. Bader partial electron charges and Wiberg bond indices were calculated using the Multiwfn software,[31] whereas the natural population analysis (NPA) scheme was used to compute partial atomic charges and spin densities with the NBO software.[32]

2.3 Interpretation of the magnetic deflection profiles

In a Stern–Gerlach experiment, a beam of atoms splits in $2J + 1$ beamlets.[33] Here, J is the total electronic angular momentum quantum number. By applying this well established behaviour to atomic yttrium deflections, the magnetic field gradient, $\delta_z B$, was determined. The latter is needed to determine the relation between the z-component of the magnetic moment, μ_z, and the deflection, d, of a particle in the experimental setup. By applying the expression for the force on a magnetic dipole in a magnetic field[34] to a cluster in the setup, it is found that:

$$d = \frac{\mu_z \delta_z B}{m v_x}\left(\frac{C_1}{v_x} + C_2\sqrt{m}\right) \qquad (1)$$

$$= c_m \mu_z, \qquad (2)$$

with C_1 and C_2 setup constants, and c_m a constant that only depends on the mass m of the cluster, because the experiment is configured in such a way that all clusters have the same velocity v_x. The magnetisation M is here defined as the expectation value of $\langle \mu_z \rangle$, the latter being an averaged projection of the magnetic moment during the interaction with the magnetic field. The broadening of a beam profile upon interaction with the magnetic field can be quantified as:

$$b = \sqrt{\sigma_{on}^2 - \sigma_{off}^2}, \qquad (3)$$

with σ_{on} and σ_{off} the variance of the concerned beam profile when the magnet is on and off, respectively.

In contrast to atoms and apart from the trivial case of being non-magnetic, the response of a cluster to a magnetic field can manifest itself in a variety of observed deflection profiles. In the following, we will discuss two models able to describe the responses of the studied clusters. It is also worth mentioning that for specific clusters with one magnetic atom in a non-magnetic host an atom-like behaviour has been observed,[35] giving rise to discrete or overlapping beamlets, and combinations of all described responses are possible as well.[36]

On the one hand, spin-rotation coupling can destroy spin quantisation through avoided crossings.[36,37] The avoided-crossing model (ACM) proposes an explanation for the most frequently observed case of a single sided deflection (SSD) towards the high field pole, resulting from the ability of the magnetic moment to rotate in the field direction. The description also holds at low temperatures where traditional vibrational behaviour no longer applies. This model ascribes single sided deflections to different energy levels in the rotation-Zeeman diagram developing more uniform slopes with increasing magnetic fields. The negative of the slope corresponds to $\mu_z = -\delta E/\delta B$ associated with an energy level with energy E in a magnetic field B. Thermal population of energy levels with slightly different slopes in the rotation-Zeeman diagram can cause an accompanied broadening of the deflection profile. Another possible cause of broadening is the variation in sensed magnetic fields as discussed further below. For low $\mu_z B$ but sufficiently high magnetic fields for the energy level slopes to reach the linearly decreasing regime in the rotation-Zeeman diagram, it is found that the magnetisation can be approximated by the Curie law:[37]

$$M = \frac{\mu_{Curie}^2 B}{3 k_B T}, \qquad (4)$$

with T the ensemble temperature of the cluster beam, and μ_{Curie} an effective magnetic moment, referring to the maximal projection of the magnetic moment in the field direction. Care has been taken to make a proper estimate of the magnetic field, by calculating an effective magnetic field as an average over each individual cluster path inside the magnet (see ESI†). Indeed, because of the field gradient, the magnetic field will vary along the curved path of a cluster inside the magnet and this curving depends on the position of the cluster in the molecular beam. From a reconstruction of the cluster path inside the magnet for all clusters (see ESI†), the mean effective magnetic field is about 0.92 T and the sensed variation in magnetic field was estimated to range from 0.01 T to 0.17 T. This latter small range of magnetic fields sensed by different clusters of the same stoichiometry consitutes another possible cause of broadening. We emphasize that to date the exact relationship between the magnetisation and magnitude of the magnetic moment is unknown. Hence, there is insufficient ground to use the Curie law for deducing exact values of magnetic moments from magnetic deflection experiments. Since this approach has been used widely in literature, it however does allow comparing results of different studies using different experimental setups. Furthermore, relative values are more trustworthy, allowing for

evaluating the evolution of the magnetic moments as function of size and composition.

On the other hand, magnetic anisotropy can cause the magnetic moment to be strongly locked to the geometry of the cluster. In this case the magnetic moment rotates with the cluster as a whole and the magnetic field only broadens the beam profile without net deflection. In terms of the ACM, this behaviour could be treated as a case where some, but not all, crossings are avoided. Although in principle the avoided-crossing model is a suitable theory to interpret the complex nature of any deflection profile, we lack the information to properly construct the rotation-Zeeman diagram. Because of this, we quantify this response using the adiabatic rigid rotor model (ARRM),[38–40] treating the clusters as a canonical ensemble of rigid spherical rotors at a rotational temperature T_{rot}. In this model, the magnitude of the magnetic moment, μ, can be estimated for weak magnetic fields, i.e. $\mu_B \ll k_B T_{rot}$, as follows. The distribution of μ_z is given by:

$$P(\mu_z) = \frac{1}{2\mu} \ln\left(\frac{\mu}{|\mu_z|}\right). \quad (5)$$

Taking into account eqn (2), and denoting by $p_{on}(z)$ and $p_{off}(z)$ the measured beam profiles for the case the magnet is on and off, respectively, the model predicts the magnet-on profile to be calculated as a convolution:

$$p_{on}(z) = \sum_{\mu_z=-\mu}^{+\mu} P^*(\mu_z) p_{off}(z - c_m \mu_z) \Delta\mu_z, \quad (6)$$

with $P^*(\mu_z)$ a normalized version of eqn (5) and $\Delta\mu_z$ the stepsize between successive μ_z values. Eventually, the magnetic moment μ_{ARRM} is found as the value of μ that minimizes the least squares deviation between the measured and calculated on profiles. Like the magnetic moment in eqn (4), the magnetic moment obtained by means of the ARRM model is also an effective magnetic moment.

3 Results

3.1 Mass spectrum

The cluster source produces a distribution of clusters of different sizes and compositions, allowing the determination of magnetic properties for different species simultaneously under the same experimental conditions. However, because of mass overlap between different compositions, not all sizes can be readily identified. Here, we studied Co_nO_m ($n = 5–18$) clusters in the 280–1200 u range (Fig. 1). The production conditions were optimized to have the highest intensities for cobalt suboxides, i.e. $m \leq n$, where $m = 0–10$. Two datasets were measured with different oxygen to cobalt ratios in the source. All other experimental conditions were the same. The dataset for the series with $n = 5–10$ was obtained for a relative lower oxygen content than the dataset for the series with $n = 11–18$.

Care was taken in the identification process by ensuring no or minimal estimated overlap in the mass spectrum with neighbouring sizes. Knowing that the mass difference between
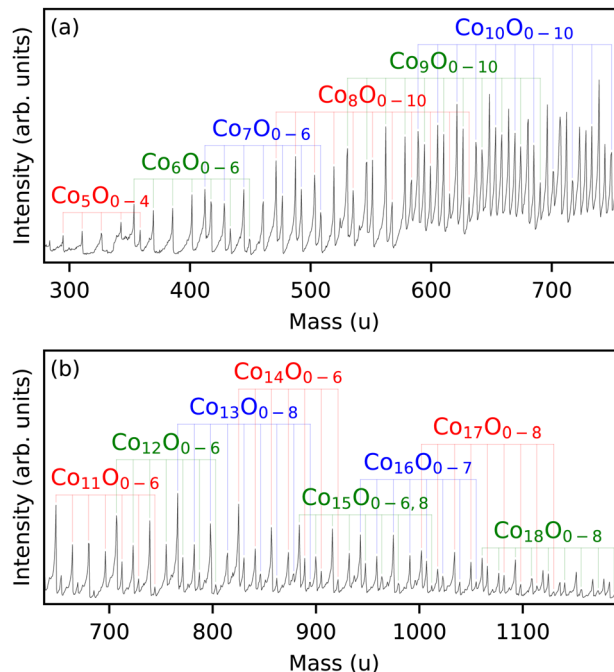

Fig. 1 Mass spectrum of the Co_nO_m clusters in (a) the 280–750 u and (b) 650–1200 u ranges. The identified clusters are labelled.

Co_3 and O_{11} is slightly less than 1 u, overlap can arise between Co_nO_m and $Co_{n-3}O_{m+11}$. For all identified sizes in Fig. 1, minimal estimated overlap was guaranteed by considering only those n values for which the average integrated intensity of $Co_{n-3}O_{8,9,10}$ is only a small percentage of the one of $Co_nO_{0,1}$. This assures that the $Co_{n-3}O_m$ clusters with $m \geq 11$ don't significantly contaminate the Co_nO_m $m \leq 10$ intensities. For $n = 5–9$ this overlap is zero, for $n = 10–18$ it is less than about 15%.

3.2 Velocity distributions and temperature

To study the evolution of magnetism as a function of stoichiometry, a properly thermalized source is required. Hereto we measured the velocity distributions[26] prior to the actual deflection experiment. Intensity distributions are measured by selecting different chopper wheel and postionisation timings and hence transmitted velocities. Examples of velocity distributions are shown in Fig. 2a and b. As described in ref. 26, such a distribution $f(v_x)$ can be modelled by:

$$f(v_x) = A \exp\left(-\frac{(v_x - w)^2}{v_{w,x}^2}\right), \quad (7)$$

with A a proportionality constant, w the cluster's flow velocity, and $v_{w,x}$ the width of the distribution given by:

$$v_{w,x} = \sqrt{\frac{2k_B T_{FF}}{m}}. \quad (8)$$

Here, T_{FF} is the translational temperature of the cluster in free flight, and m the cluster mass. Fig. 2c shows T_{FF}, obtained by fitting the velocity distribution to eqn (7), as a function of cluster mass. According to ref. 26, the observed mass
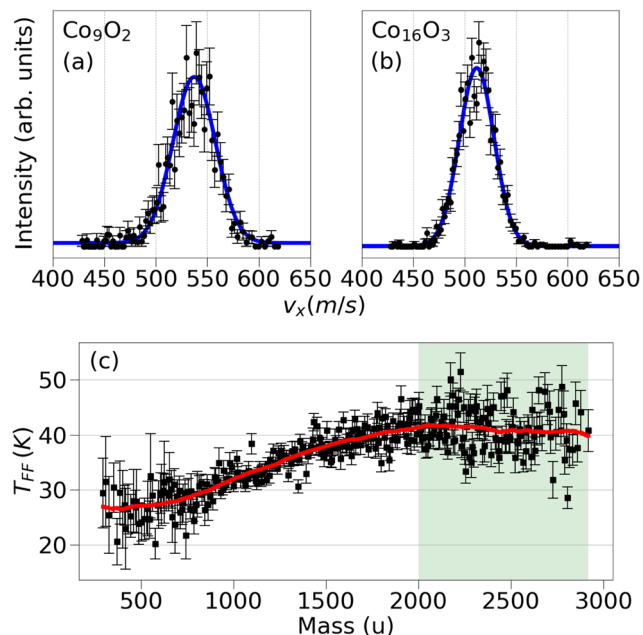
Fig. 2 Velocity distributions of (a) Co_9O_2 and (b) $Co_{16}O_3$. The blue curve corresponds to the fit function of eqn (7) (apart from a constant noise level). Clearly, most clusters of the smaller mass move faster than the ones of the heavier mass with the distributions of Co_9O_2 and $Co_{16}O_3$ displaying maxima at 537 ± 1 m s^{-1} and 511.6 ± 0.3 m s^{-1}, respectively. (c) Translational temperatures in free flight as a function of cluster mass. The shaded region corresponds to clusters with a T_{FF} converging to the source temperature. The red curve is a guide to the eye.

Fig. 3 A selection of beam profiles. The red circles and blue crosses show the measured intensities at detector positions z with and without magnetic field, respectively. The solid lines correspond to the Gaussian smoothened profiles (FWHM = 0.5 mm, same colour coding). The dashed curves represent the best suiting ARRM (if applicable). With increasing number of Co atoms, Co_nO_4 displays a small SSD ($n = 6$), a larger SSD ($n = 7$) and an ARRM-like behaviour ($n = 8$), demonstrating that the addition of one Co atom can change the response significantly. Another ARRM case was found for Co_8O_6.

dependence corresponds to the fingerprint of a thermalized source: from a certain mass, here at about 2000 u, T_{FF} converges to the temperature of the clusters in the source, which is considered to be 41 ± 4 K. Those heavier clusters experience basically no translational cooling from random collisions with the carrier gas in the expansion, because of a substantial velocity slip with respect to the carrier gas. The velocity distribution of smaller clusters, on the other hand, does overlap with that of the expanding carrier gas. Consequently, the smaller clusters experience translational cooling and have a lower T_{FF} than the source temperature. These two regions are highlighted with different background colours in Fig. 2c.

3.3 Magnetism

A selection of measured beam profiles is shown in Fig. 3. Beam profiles of all studied Co_nO_m clusters are available in the ESI† Fig. S3–S5. Most beam profiles in our experiment display an SSD, although five clusters show signs of locked moment behaviour, *i.e.* Co_5O_1, Co_5O_3, Co_7O_5, Co_8O_4, and Co_8O_6. The measured magnetic moments obtained by means of the Curie law and ARRM are presented in Fig. 4, together with the broadenings computed according to eqn (3). When discussing tendencies involving μ_{Curie}, systematic uncertainties are left out. Systematic uncertainties originate from uncertainties in the determination of the magnetic field, the temperature of the clusters inside the source, atomic deflection calibration parameters and setup constants. Non-systematic uncertainties arise
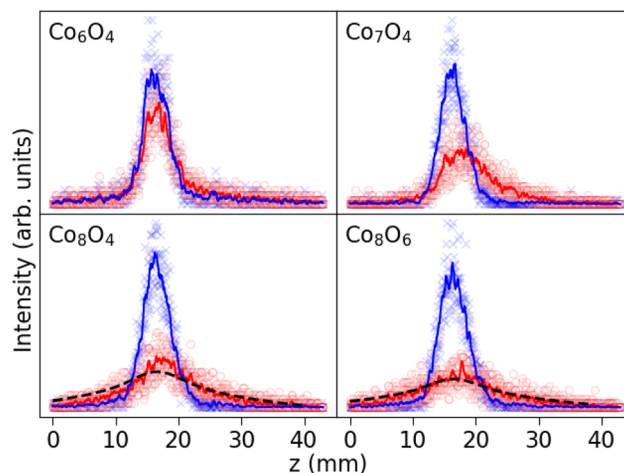
only from the discrete Poisson-distributed counts on the position channels of the detector. Systematic uncertainties on μ_{Curie} are for most clusters in the range of 1–2 μ_B. This value does not incorporate the model uncertainty on the use of the Curie law, which as discussed below is the largest unknown.

It is important to recognize that the application of both the Curie law and ARRM has some restrictions. On the one hand, asymmetric broadenings in the deflected beam profiles normally occur if the ARRM weak field condition is not satisfied, an effect that becomes stronger with increasing magnetic fields.[39,40] In the present study, the set of clusters showing ARRM behaviour display a vanishingly small to noticeable deflection towards the high field pole, while strictly speaking no net deflection is expected. Because all ARRM deflection profiles are reasonably well symmetric, we consider the above procedure to extract the ARRM magnetic moments by the application of eqn (6) still reliable. On the other hand, while the ACM is appropriate for all cluster sizes and temperature regimes, the applicability of the Curie law emerging from the model is not straightforward. It is more appropriate to examine the variation of magnetism with cluster stoichiometry, rather than the absolute values of the magnetic moments. Secondly, the avoided-crossing model was derived for ferromagnetic pure cobalt clusters ignoring the orbital contribution to the magnetism.[37] Orbital quenching is a good approximation for bulk first row transition metals[41] and for bulk cobalt, the latter having an orbital magnetic moment per atom μ_L that is only about 10% of its spin magnetic moment per atom μ_S.[42,43] In contrast, X-ray magnetic circular dichroism (XMCD) studies of singly-ionized Co_n^+ clusters reveal that, for the size range of the experiment, the orbital contribution to the magnetic moment per atom is significant, but generally diminishes with increasing
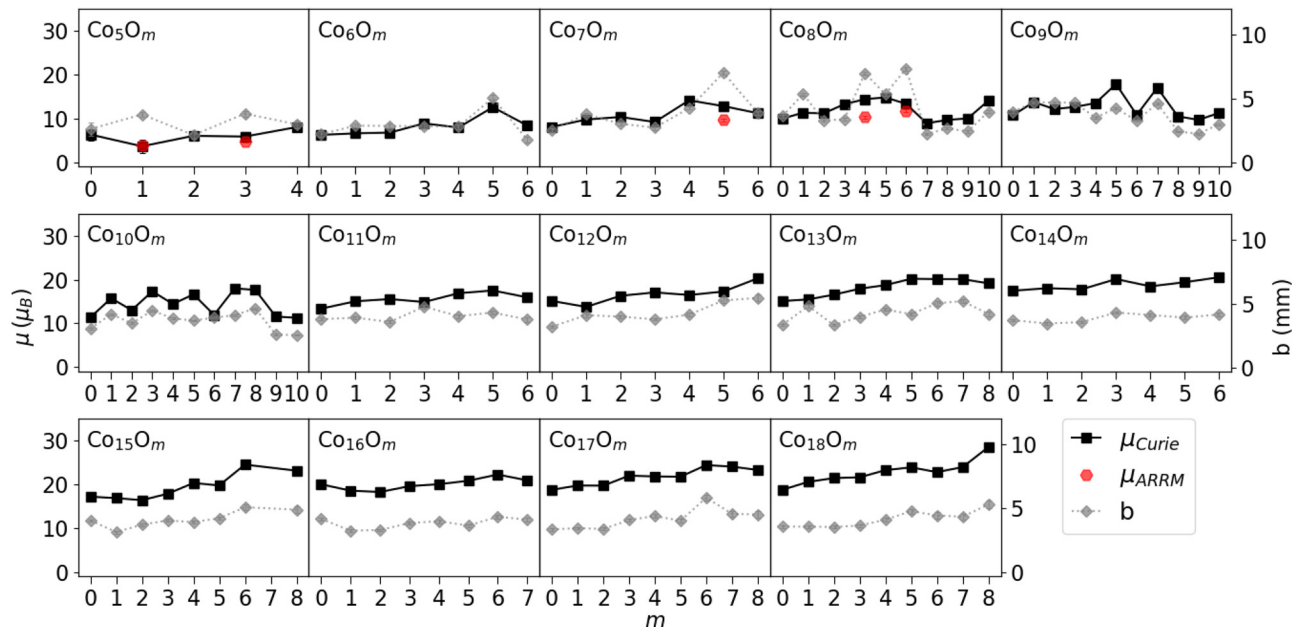
This journal is © the Owner Societies 2023

Phys. Chem. Chem. Phys., 2023, **25**, 171–182 | **175**

Fig. 4 Experimentally determined total magnetic moments calculated by means of the Curie law (μ_{Curie}) and adiabatic rigid rotor model (μ_{ARRM}), and broadenings (*b*) for all Co_n oxide series. Rather than providing absolute values, the Curie law was used to study the evolution of the magnetism with oxygen content. Hence, systematic uncertainties on μ_{Curie} have been omitted. Remaining uncertainties for all displayed quantities are relatively small and mostly not visible. Random uncertainties on μ_{Curie} typically range from $0.2\mu_B$ to $0.7\mu_B$, and from 0.1 mm to 0.2 mm for *b*.

cluster size.[44,45] These studies quote μ_L/μ_S ratios from about 60% for $n = 5$ to about 25% for $n = 17$. To our knowledge, no results have been reported about the orbital contributions in the corresponding cobalt oxide clusters. Furthermore, an adequate estimation of the temperature that should be used in the Curie law is challenging. The total magnetic moments determined by means of the Curie law in Fig. 4 are calculated for the case the population of all energy levels is stagnant upon exiting the source. Because we have a well thermalized source, as explained above, this is equivalent of using the source temperature as the relevant temperature. In reality though, the relevant temperature in the Curie law might be subject to cooling effects, meaning that the obtained values for μ_{Curie} are upper limits.

From Fig. 4, some conclusions can be drawn. (1) With increasing number of cobalt atoms, the clusters become more magnetic. This is in line with the ferromagnetic nature of macroscopic Co and pure Co clusters.[37,41,46] (2) Overall there is also a tendency of increasing magnetic moment with increasing number of oxygen atoms. For the smaller Co_nO_m clusters with $n = 5$–10, μ_{Curie} displays fluctuations as a function of m, but the increasing trend is noticeable for $n = 5$–8. A clear odd-even staggering is present in the Co_9O_m ($m = 4$–8) and $Co_{10}O_m$ ($m = 0$–7) series with higher magnetic moments for clusters with an odd number of oxygen atoms. For $n = 11$–18 the magnetic moment increases almost monotonically with the number of oxygen atoms. (3) For most clusters, the broadening is in the range from 2.0 to 5.5 mm, except in 3 noticeable cases: Co_7O_5, Co_8O_4, and Co_8O_6, whose deflection profiles are classified as rigid rotor behaviour. All broadenings are significantly greater than zero, which implies a magnetic response of all

studied clusters. There is no clear increase in broadening with n as is the case for the magnetic moment, although on average the broadenings are relatively lower in the $Co_{5,6}O_m$ series as compared to the rest. Mostly the broadening for all series in Fig. 4 closely resembles the trends in μ_{Curie} as a function of m. Remarkable exceptions are the clusters with identified ARRM response, which have a broader deflection profile than the neighbouring clusters. (4) Despite the limitations in applicability, discussed in the previous paragraph, the Curie law and ARRM yield similar magnetic moment values. Because of the different ways these magnetic moments were obtained, this correspondence is reassuring for both methods to deduce the presented values. Moreover, in all rigid rotor cases $\mu_{\text{Curie}} \gtrsim \mu_{\text{ARRM}}$, which is consistent with the idea that the calculated μ_{Curie} values provide an upper limit. Observations (1) and (2) will be explored in more detail in the discussion section, taking also into account the results of the DFT calculations.

The investigated species include the $Co_{13}O_8$ system, which was reported to have a special stability and a high magnetic moment by Geng *et al.*[24] We found no particularly high intensity for this cluster in the mass spectrum, nor an enhanced magnetic moment compared to other members of the $Co_{13}O_m$ series. The total effective magnetic moment of $Co_{13}O_8$, calculated by means of the Curie law, is 19 ± 2 μ_B, about 65% of the effective total spin magnetic moment (about 29 μ_B) computed by Geng *et al.*[24]

3.4 DFT calculations

In order to get a more qualitative insight into the mechanism that is responsible of producing the observed trends in magnetic moment, especially the increasing magnetism with the

176 | *Phys. Chem. Chem. Phys.*, 2023, **25**, 171–182

This journal is © the Owner Societies 2023

addition of oxygen, we investigated the Co_6O_m (m = 0, 4, 5, 6) and Co_7O_m (m = 0, 3, 4, 5) series computationally. These size ranges were chosen because the experiments revealed a strong oxygen concentration dependence with a local maximum in μ at m = 5 and 4 for the Co_6O_m and Co_7O_m series, respectively. We must emphasize that the DFT calculations presented here only take into account the spin contribution to the magnetic moment, in addition to the intrinsic assumption that the wavefunctions of the clusters can be described by a single configuration.[47] Experimentally, though, total magnetic moments, estimated by μ_{Curie} and μ_{ARRM}, are obtained that cannot be decomposed into spin and orbital parts.

The strong interaction between cobalt and oxygen, also known from previous studies,[15] shows up in different properties of the clusters. First, the lowest energy structures of all calculated clusters (presented in Fig. 5) have a large number of Co–O bonds. More specifically, in the case of Co_6O_m, it was found that the oxygen atoms adopt positions with a high Co coordination. Geometries where two oxygens coordinate directly are not stable. For the Co_7O_m series, the lowest energy geometries of the clusters show that all oxygen atoms adopt threefold Co-coordinated sites. Second, the density of states of the calculated Co_6 oxides (see ESI,† Fig. S2) reveals that the cobalt d-states strongly hybridize with the oxygen valence states. Third, Wiberg bond indices, measuring the average number of electron pairs (*i.e.* 'bonds') shared by two atoms, indicate a strong Co–O interaction. The calculated values for both series can be found in ESI,† Tables S2 and S4. Although there is notable spread on the calculated bond indices, some general characteristics are observed. With the exception of one cobalt atom in Co_7O_3, all other cobalt atoms are bound to oxygen. On average, the Wiberg bond indices for Co–O bonds lie between 0.7 and 0.8 for Co_6O_m, and between 0.8 and 0.9 for Co_7O_m, reflecting the formation of single bonds. In general, the pairs of adjacent Co atoms have Wiberg bond indices around 0.56 for Co_6, but those values decrease to 0.26, 0.23, and 0.33

for Co_6O_m with m = 4, 5, and 6 respectively. In the case of Co_7O_m, these Co–Co indices also decrease on average from 0.41 for pure Co_7, to 0.30, 0.27, and 0.24 for m = 3, 4, and 5 respectively. Solely for three Co–Co pairs in Co_7O_3, of which only one cobalt atom is bound to oxygen, the Co–Co index increases to 0.60. In general, the Wiberg bond indices indicate that oxygen interacts more strongly with Co in comparison with the interaction between Co pairs and also weakens the cobalt–cobalt interaction. Also they suggest that metal–metal bonds survive in the oxidized clusters and this could be an important reason for why the magnetism survives in the studied clusters.

Partial charge analysis reveals a major charge redistribution in the clusters due to the presence of oxygen. Partial charges in a molecular system depend to a large extent on the method employed to define such a partial charge, because partial charge is not a quantum observable. Here, three methods were employed in order to corroborate the consistency of results, namely the Löwdin, NPA, and Bader schemes. The partial electron charges for all calculated $Co_{6,7}O_m$ clusters according to the three schemes can be found in the ESI,† (Tables S1 and S3). Qualitatively, similar results are obtained for all schemes. All three methods indicate that oxygen accepts electrons from cobalt. This can for example be inferred from Table 1 showing the local partial electron charges for the $Co_{6,7}O_m$ clusters using the Bader scheme. Although, on average, the Bader and Löwdin scheme for Co_6O_m predicts the largest transfer for the m = 5 cluster, which was experimentally found to possess the largest magnetic moment in the m = 0–6 series, the general trend for Co_6O_m and Co_7O_m is an increasing amount of charge transfer for increasing oxygen content.

The calculated total spin magnetic moment μ_s for the lowest energy configuration of Co_6 is 14 μ_B, a value that increases to 16 μ_B for Co_6O_4 and to 18 μ_B for Co_6O_5. For Co_6O_6, it decreases to 16 μ_B. In the Co_7O_m series, the obtained values are 15, 15, 17, and 15 μ_B, for Co_7, Co_7O_3, Co_7O_4, and Co_7O_5, respectively. Qualitatively, all these trends are consistent with the experimental observations.

Fig. 6 compares the computed spin magnetic moments in this work with the ones from a previous study of Aguilera-del-Toro *et al.*[20] The experimental magnetic moments are also included to qualitatively compare the calculated and measured
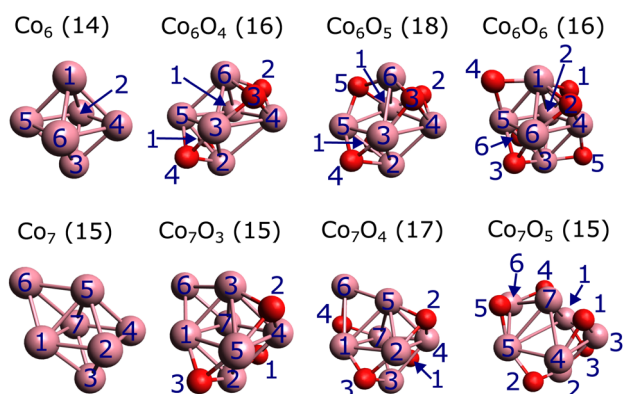

Fig. 5 Lowest-energy geometries of the Co_6O_m (m = 0, 4, 5, 6) and Co_7O_m (m = 0, 3, 4, 5) clusters, calculated at the PBE0/def2-TZVP level. The associated computed total spin magnetic moments μ_s in Bohr magnetons are shown in parenthesis. The labels of the cobalt (purple) and oxygen (red) atoms correspond to the designations in Tables 1 and 2, and in the ESI,† Tables S1–S4.

Table 1 Partial electron charges (in units of the elementary electric charge e) of the different atoms (labeled according to Fig. 5) in Co_6O_m (m = 0, 4–6) and Co_7O_m (m = 0, 3–5) using the Bader scheme

	Co_6	Co_6O_4	Co_6O_5	Co_6O_6	Co_7	Co_7O_3	Co_7O_4	Co_7O_5
Co(1)	−0.01	0.83	1.22	1.01	0.01	0.40	0.76	0.77
Co(2)	0.01	0.84	0.77	0.84	−0.01	0.69	0.73	0.75
Co(3)	−0.01	0.83	0.88	1.05	−0.00	0.46	0.70	0.84
Co(4)	0.00	0.91	0.76	0.98	−0.01	0.82	0.79	0.71
Co(5)	0.00	0.66	1.21	0.96	−0.02	0.71	0.53	0.77
Co(6)	0.01	0.65	1.21	0.87	0.02	0.49	0.34	0.85
Co(7)	—	—	—	—	0.02	−0.11	0.86	1.15
O(1)	—	−1.18	−1.21	−0.96	—	−1.15	−1.17	−1.19
O(2)	—	−1.18	−1.21	−0.96	—	−1.16	−1.17	−1.18
O(3)	—	−1.18	−1.20	−1.00	—	−1.17	−1.16	−1.18
O(4)	—	−1.18	−1.21	−0.99	—	—	−1.20	−1.16
O(5)	—	—	−1.22	−0.92	—	—	—	−1.13
O(6)	—	—	—	−0.89	—	—	—	—

This journal is © the Owner Societies 2023

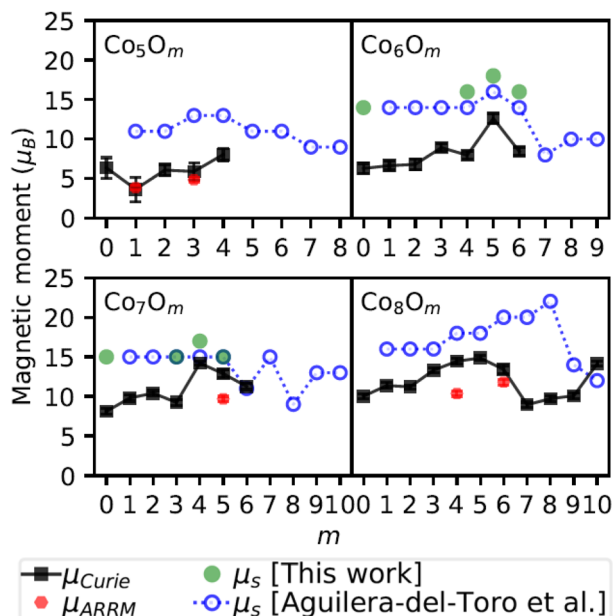*Phys. Chem. Chem. Phys.*, 2023, **25**, 171–182 | **177**

Fig. 6 Comparison between the experimental effective total magnetic moments μ_{Curie} and μ_{ARRM}, and the calculated total spin magnetic moments, $2S\mu_B$, with S the total spin quantum number, obtained in this work and by Aguilera-del-Toro et al.[20] for the lowest energy structures of the neutral Co_nO_m clusters in the range n = 5–8. All magnetic moment values are in Bohr magnetons. Systematic uncertainties on μ_{Curie} are not included in the error bars.

Table 2 Local spin magnetic moments μ_s in μ_B of the different atoms (labeled according to Fig. 5) in Co_6O_m (m = 0, 4–6) and Co_7O_m (m = 0, 3–5) using the natural orbital decomposition

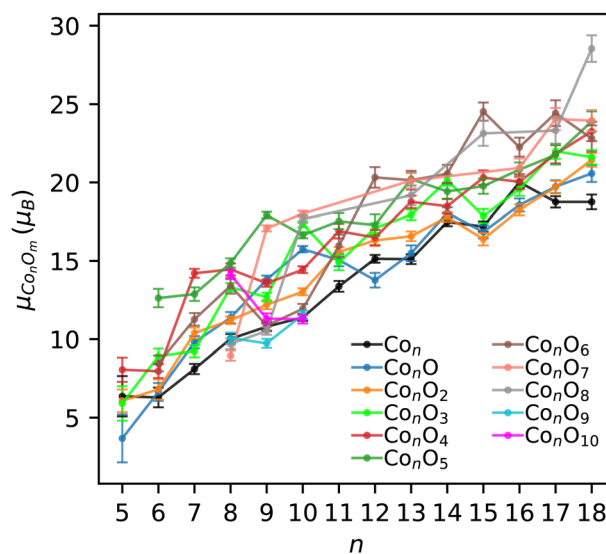|	Co_6	Co_6O_4	Co_6O_5	Co_6O_6	Co_7	Co_7O_3	Co_7O_4	Co_7O_5
Co(1)	2.33	2.27	2.65	2.55	2.05	1.94	2.11	2.14
Co(2)	2.34	2.25	2.90	2.53	2.16	2.07	2.11	2.10
Co(3)	2.33	2.27	2.35	2.57	2.46	2.05	2.07	2.29
Co(4)	2.34	2.34	2.92	1.17	2.20	2.26	2.21	2.07
Co(5)	2.34	2.78	2.66	2.51	2.10	2.07	2.52	2.15
Co(6)	2.34	2.77	2.63	2.51	1.97	2.08	2.60	0.70
Co(7)	—	—	—	—	2.06	1.82	2.25	2.53
O(1)	—	0.34	0.42	0.25	—	0.28	0.25	0.23
O(2)	—	0.32	0.42	0.30	—	0.22	0.24	0.26
O(3)	—	0.32	0.35	0.41	—	0.22	0.29	0.22
O(4)	—	0.34	0.33	0.39	—	—	0.33	0.11
O(5)	—	—	0.37	0.56	—	—	—	0.18
O(6)	—	—	—	0.25	—	—	—	—

Fig. 7 Experimental total magnetic moments determined by the Curie law for the Co_nO_m clusters, grouped by amount of oxygen atoms, as a function of n. Systematic uncertainties are not included in the error bars.

trends as a function of oxygen content. Quantitative comparison between the computed and experimental values is not appropriate because of the different contributions to the concerned magnetic moments. There is a good correspondence between our calculated spin magnetic moments and the ones from ref. 20. In particular, both calculations predict Co_6O_5 to have a slightly larger spin magnetic moment than its immediate neighbours, with the values in this work to be consistently 2 μ_B larger than the ones obtained by Aguilera-del-Toro et al.[20] For the Co_7O_m series, apart from m = 4, the exact same values are obtained in our work and ref. 20. In general, the experimental magnetic moments are significantly smaller than the predicted ones. Overall though, the theoretically obtained trends agree well with the progression of μ_{Curie} for growing m, except for $Co_7O_{m \geq 4}$ and $Co_8O_{m \geq 6}$.

In order to explore the agreement between the experimental results and our calculations further, natural electron configurations per atom were computed using the natural orbital decomposition. The results can be retrieved from the ESI,† Tables S5–S12. From these natural electron configurations, local spin magnetic moments were derived. Table 2 lists the calculated μ_s values per atom for the $Co_{6,7}O_m$ series, that will be discussed below.

4 Discussion

An indication of the ferromagnetic nature of the Co_nO_m clusters was already provided in Fig. 4. This aspect can be inferred

further from Fig. 7, showing the experimental total magnetic moments of all Co_nO_m clusters as a function of the number of cobalt atoms n. The m = 9 and 10 series only contain three points, which is too little to observe a distinctive trend. All other fixed-m series display a clear tendency of increasing magnetic moments with growing n. This trend implies a ferromagnetic coupling between the cobalt atoms, both in the pure and oxidized cobalt clusters. This is consistent with the ferromagnetic nature of pure Co_n clusters reported in ref. 37, 46, 48–50.

Before investigating the experimental data in more detail, it is instructive to first elaborate on the computational results of the natural orbital decomposition for the eight selected $Co_{6,7}O_m$ clusters. These findings will then be used to provide further insight in the interpretation of the measured magnetic moments. Outcomes of this DFT analysis are presented in Fig. 8 for Co_6O_4 and Co_7O_4. Population analysis revealed that in both the pure and oxidized $Co_{6,7}O_m$ clusters, the local cobalt

178 | Phys. Chem. Chem. Phys., 2023, **25**, 171–182
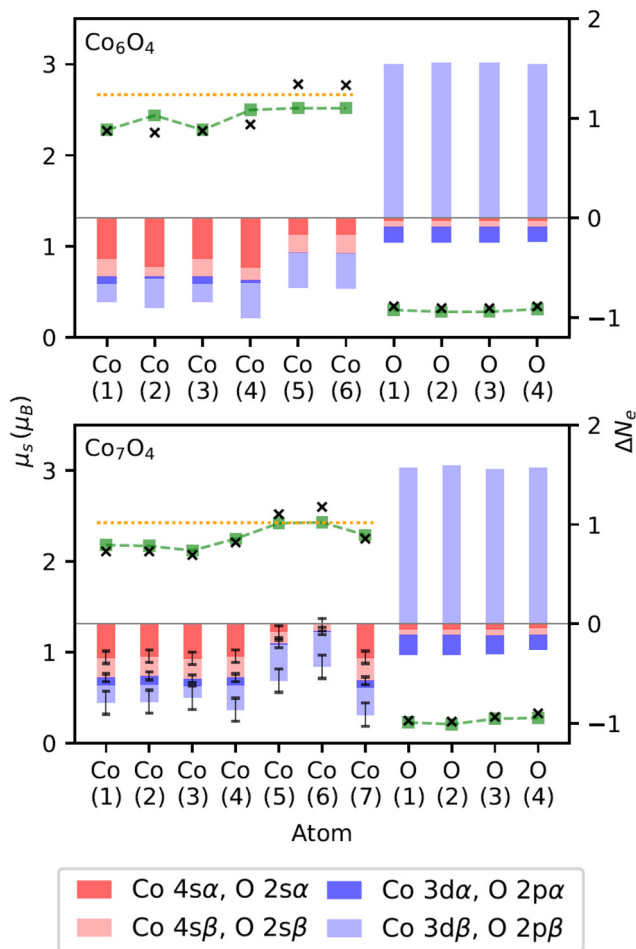
This journal is © the Owner Societies 2023

Fig. 8 Magnetic and orbital characteristics for each atom (labeled according to Fig. 5) in Co_6O_4 and Co_7O_4, resulting from the natural orbital decomposition. The black crosses are the total spin magnetic moments, μ_s, of the respective atoms (left scale). The green dashed curves depict the local μ_s values obtained by only taking into account the cobalt 3d electrons and oxygen 2p electrons for the cobalt and oxygen atoms, respectively. Marked by the orange dotted line is the value of the average μ_s per cobalt atom, calculated as the total spin magnetic moment of the cluster divided by the number of cobalt atoms. The red and blue bars visualize the change in the number of electrons per orbital type and spin orientation (see legend) upon oxidation. Each population change, ΔN_e, represents a decreasing (negative) or increasing (positive) number of electrons with respect to the corresponding reference (see text). The height of each bar in the stack corresponds with the actual ΔN_e value (right scale). Uncertainties on ΔN_e (see text) smaller than 0.01 are not shown for better viewing.

magnetic moments are mainly caused by the 3d electrons. There is a smaller contribution of the 4s electrons that can be either parallel or antiparallel with respect to the 3d levels. On average, the 4s spin moments contribute about 4% to the local cobalt magnetic moment, but there are some atoms where the 4s electrons contribute between 0.1 and 0.3 μ_B. The net cobalt 4s magnetic moment, also found to be either positive or negative, was determined to be on average 3% of the total cluster's magnetic moment. The electronic ground state configuration of the free cobalt atom is $[Ar]3d^7 4s^2$. Following

Hunds rules, there are three unpaired electrons in the 3d subshell. In general, the cobalt atoms in the computationally investigated clusters have a decreased spin magnetic moment in comparison with the corresponding value of 3 μ_B of the free cobalt atom.

The local spin magnetic moments of the oxygen atoms are nearly entirely due to the 2p orbitals. In all computationally investigated clusters, the oxygen spin magnetic moments are much lower than the corresponding value of 2.0 μ_B of the free oxygen atom. From the calculated μ_s values for the selected $Co_{6,7}O_m$ clusters with $m > 0$ (see Table 2), it was derived that the mean spin magnetic moment per oxygen atom is about 13% of the mean spin magnetic moment per cobalt atom. With respect to the entire cluster, the net contribution of oxygen to the total magnetic moment is found to be 6% on average. These numbers suggest a non-negligible, but rather small contribution of oxygen to the value of the total spin magnetic moment, $\mu_{s,tot}$, of the examined clusters. Consequently, with n representing the number of cobalt atoms in a cluster, the value of $\mu_{s,tot}/n$, portrayed by the orange dotted line in Fig. 8, in general gives a good first order estimation of the local cobalt magnetic moments.

In agreement with the experimental findings, all local cobalt spin magnetic moments align parallel, implying a ferromagnetic coupling between them both in the pure and oxidized clusters. Also the spin magnetic moments of all oxygen atoms are oriented parallel with those of the cobalt atoms.

Apart from two exceptions, the DFT calculations indicate that the cobalt atoms in the investigated clusters populate their 3d orbitals analogously to Hund's first rule, with about 5 electrons of α-spin in all cobalt 3d orbitals. We will refer to this observation of maximizing the 3d spin in the discussion of the experimental results. As evidenced by the previous discussion of the local cobalt magnetic moments, there are more 3d electrons of β-spin for the cobalt atoms in the clusters than in the free cobalt atom. On the contrary, the occupation of the cobalt 4s orbitals in all clusters is lower than in the free cobalt atom for both spin orientations.

We also examined the effect of oxidation on the population of the cobalt 4s and 3d orbitals, and the oxygen 2s and 2p orbitals of the selected $Co_{6,7}O_m$ clusters. Hereto, we calculated the population changes, ΔN_e, for these orbitals upon oxidation, where N_e denotes the number of electrons of one particular spin in one particular orbital type. The results are presented in Fig. 8. For every cobalt or oxygen atom in the oxidized Co_nO_m clusters, each ΔN_e resembles the difference in N_e for that atom with respect to the corresponding value averaged over all cobalt atoms in the associated pure Co_n cluster or for the free oxygen atom, respectively. While there is almost no variation in local N_e values of the 4s and 3d orbitals for both spin orientations over the constituent cobalt atoms in Co_6, there is notable spread on the average N_e values of Co 4sα, Co 4sβ, and Co 3dβ in the case of Co_7. This spread is the cause of the error bars in Fig. 8. In general upon oxidation, a decreasing N_e is noticed for the cobalt atoms in the oxidized clusters for 4s electrons of both spin orientations and also for 3d electrons of β-spin.

This journal is © the Owner Societies 2023

Phys. Chem. Chem. Phys., 2023, **25**, 171–182 | **179**

The amount of 3d electrons of α-spin remains almost unchanged. With respect to the free oxygen atom, we see a large increase in oxygen 2p electrons of β-spin, but a similar number of oxygen 2p electrons of α-spin and oxygen 2s electrons of both spin orientations.

The analysis of the population changes not only shows that there is charge transfer from cobalt to oxygen upon oxidation, but also suggests that this transfer arises from the cobalt 3d and 4s valence orbitals to oxygen 2p β orbitals. While cobalt 4s electrons of both spin orientations are involved in the transfer, the electron donation from the cobalt 3d states emanates mainly from the β orbitals. These transfers determine the magnetic response of an oxidized cluster. We will further interpret the influence of oxygen on the magnetism of the experimentally studied clusters, by adhering to this mechanism arising from the DFT calculations.

The experimental magnetic moments per number of cobalt atoms in a cluster, $\mu_{Co_nO_m}/n$, are presented in Fig. 9 as a function of the oxygen-to-cobalt ratio m/n. Because of potential non-vanishing oxygen magnetic moments, the quantities $\mu_{Co_nO_m}/n$ do not correspond directly to the average magnetic moment of a cobalt atom in the clusters (except for pure Co_n), but since the contribution of the oxygen atoms is rather small (*cf.* DFT calculations), $\mu_{Co_nO_m}/n$ can be interpreted as a first order approximation of the local cobalt magnetic moments. Consequently, the data in Fig. 9 indicates that the magnetic moment per cobalt atom is enhanced for most oxide clusters with respect to the pure cobalt clusters and also grows larger with increasing m/n. However, it seems that a turning point arises around $m/n \approx 0.75$, where the magnetic moment per cobalt atom tends to decrease as more oxygen is added. The experimental magnetic moments per cobalt atom of the eight computationally investigated clusters are all smaller than the

corresponding mean spin magnetic moments per cobalt atom from the DFT calculations, on the average by an amount of 0.7 μ_B.

For the metallic Co_n clusters, the measured magnetic moments per cobalt atom range from 1.0 ± 0.1 μ_B for Co_{18} up to 1.3 ± 0.3 μ_B for Co_5. These values are significantly lower than the ones reported by other deflection[48,51] and theoretical[52,53] studies. Also, in contrast to these studies our values lie below the bulk value of 1.7 μ_B.[46,49,51] But it should be noted that the results of these studies do not agree well. The most probable explanation for the differences in magnetic moments derived from the deflection studies of Knickelbein[48] and Xu *et al.*,[51] but also for the differences between these two studies and this study, is likely to be the difficulty in determining the relevant temperature and precise magnetic field in the approximative Curie law. An accurate assessment of the magnetic field can indeed be complicated in practice by large applied gradients, as in this study.

To explore the data in Fig. 9 in more detail, we will only take the spin contribution to the magnetic moment into account. Furthermore, the DFT calculations imply that the cobalt 4s electrons play a minor role in the magnetism of the investigated clusters. Therefore, it is also useful to regard $\mu_{Co_nO_m}/n$ as a first order approximation of the magnetic moment per cobalt atom caused only by the 3d electrons, the actual values of which are estimated to lie within an extra uncertainty interval of 0.2 μ_B on top of the error bars in Fig. 9. We arrived at this typical additional uncertainty by considering characteristic values for the contributions of the oxygen atoms and the cobalt 4s electrons from the DFT calculations. As put forward by the DFT calculations, we will further assume that the cobalt 3d orbitals are filled by maximizing the total electron spin.

Because a single electron contributes one Bohr magneton to the total spin magnetic moment, the interpretation of Fig. 9 suggests that pure cobalt clusters have an increased 3d occupancy with respect to the free cobalt atom. Whereas the latter has 3 unpaired 3d electrons giving rise to a spin magnetic moment of 3 μ_B, all measured Co_n clusters must have less unpaired electrons in the 3d levels (corresponding to an increased 3d occupancy), in a range slightly more than one.

The initial rise in local cobalt magnetic moments with increasing oxygen-to-cobalt ratios can be explained as oxygen taking away β spin electrons from the cobalt 3d orbitals. Around the turning point, each cobalt atom has a maximal magnetic moment of about 2 μ_B, indicating that oxygen was not able to take away all 3d β spin as the latter would give the cobalt atoms a magnetic moment of 5 μ_B. Even if we incorporate a maximal uncertainty on the interpreted cobalt 3d magnetic moments of Fig. 9, estimated to be 1 μ_B on the values, the data suggests that the occupation of the cobalt 3d levels is never less than for the free cobalt atom. This is in full agreement with the findings of the DFT calculations. As a rough estimate, the oxidation process is able to maximally increase the magnetic moments of the cobalt atoms by about 1 Bohr magneton. As such, maximally about n 3d electrons are donated from the cobalt to m oxygen atoms, on average
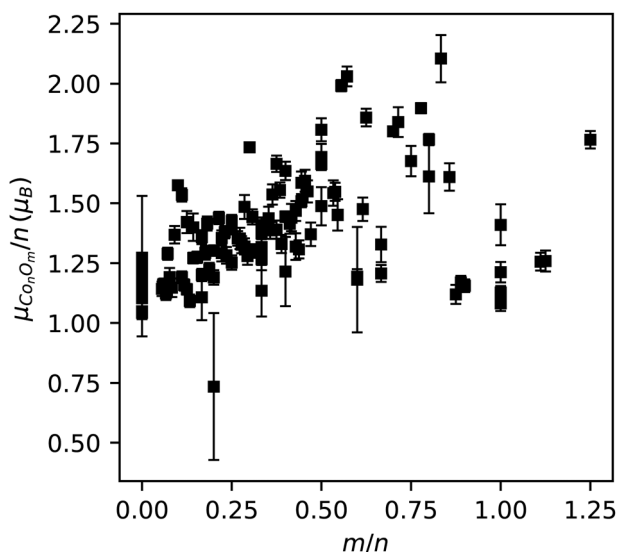
Fig. 9 Experimental magnetic moments per number of cobalt atoms in a cluster, calculated by means of the Curie law, for the Co_nO_m clusters in function of the oxygen-to-cobalt ratio m/n. Systematic uncertainties are not included in the error bars.

180 | *Phys. Chem. Chem. Phys.*, 2023, **25**, 171–182

This journal is © the Owner Societies 2023

leading to a maximal transfer of $n/m = 1/0.75 \approx 1.3$ 3d electrons to each oxygen atom.

Different types of interaction for different sizes and compositions could explain the large scattering around $m/n = 0.75$. Because of this, we can only speculate about the behaviour at oxygen-to-cobalt ratios higher than 0.75, where the magnetic moments appear to reduce. In line with our reasoning, the only possibility for this decline is a diminishing charge transfer of 3d β electrons from the cobalt to oxygen, leaving the cobalt atoms with less unpaired electrons in the 3d orbitals.

We also investigated the effect of oxygen on the local cobalt magnetic moments by considering a non-vanishing oxygen contribution. Hereto we estimated the average magnetic moment per oxygen atom to be 13% of the average magnetic moment per cobalt atom for all clusters, a percentage taken from the DFT calculations. For this situation, we obtain a very similar behaviour as the one in Fig. 9 with slightly lower magnetic moments per cobalt atom, reinforcing the evidence for the increase of the local cobalt magnetic moments with relative oxygen composition.

Similar conclusions could also be drawn for small Co oxide cations $Co_nO_m^+$ ($n = 2, 3$ and $1 \leq m \leq 4$) that were studied in ref. 54. The DFT calculations in that work also revealed an increase in the total spin magnetic moment of the Co oxide clusters as the oxygen content grows, due to an increasing number of unpaired electrons in the 3d4s shell of the cobalt atoms accompanied with the donation of electrons to atomic oxygen bonds by a cobalt atom.

5 Conclusions

A Stern–Gerlach magnetic deflection experiment has been conducted on neutral gas phase Co_nO_m ($n = 5$–18 and $m = 0$–10) clusters, produced by laser ablation and gas aggregation. In addition, DFT calculations of structural, electronic, and magnetic properties have been performed for a selection of $Co_{6,7}O_m$ clusters.

Experimentally, we found evidence for ferromagnetic coupling between the cobalt atoms both in the pure cobalt clusters and in their oxidized counterparts, with oxygen reinforcing the ferromagnetic coupling between the cobalt atoms. The magnetic moment per cobalt atom in the oxidized clusters is, for most clusters, enhanced with respect to the pure cobalt clusters and largely displays an increasing tendency with growing relative oxygen content.

The DFT calculations confirm the ferromagnetic coupling between the cobalt atoms in the pure and oxidized cobalt clusters. In addition, the small spin magnetic moments on the oxygen atoms were found to align parallel with Co in all calculated clusters. The computations demonstrate an increased 3d level population per cobalt atom with respect to the free cobalt atom for all investigated clusters. This is consistent with the discussion of the experimental results. We found a qualitative agreement between the trends of the predicted and measured total cluster magnetic moments, although they do not agree quantitatively.

The following mechanism was proposed to explain the magnetism of the studied clusters. Both in the pure and oxidized cobalt clusters the magnetic response is mainly determined by the cobalt 3d electrons, and to a much lesser extent by the cobalt 4s and oxygen 2p orbitals. Upon oxidation, there is electron transfer from the 3d and 4s valence states of the cobalt atoms to oxygen. The cobalt 3d orbitals donate mainly electrons of minority spin, but there is no spin preference towards emptying the cobalt 4s states. The different occupations of the energy levels taking part in this transfer cause the size-to-size variations in cluster magnetic moments.

Conflicts of interest

There are no conflicts to declare.

Acknowledgements

References

1 F. Hasannezhad, L. Naji and M. Arvand, *Mater. Sci. Semicond. Process.*, 2022, **139**, 106333.

2 A. Raghunath and E. Perumal, *Int. J. Antimicrob. Agents*, 2017, **49**, 137–152.

3 K. Kalantar-zadeh, J. Z. Ou, T. Daeneke, A. Mitchell, T. Sasaki and M. S. Fuhrer, *Appl. Mater. Today*, 2016, **5**, 73–89.

4 H. Osgood, S. V. Devaguptapu, H. Xu, J. Cho and G. Wu, *Nano Today*, 2016, **11**, 601–625.

5 S. Lee, A. Halder, G. A. Ferguson, S. Seifert, R. E. Winans, D. Teschner, R. Schlögl, V. Papaefthimiou, J. Greeley, L. A. Curtiss and S. Vajda, *Nat. Commun.*, 2019, **10**, 954.

6 J. Park, X. Shen and G. Wang, *Sens. Actuators, B*, 2009, **136**, 494–498.

7 V. Skumryev, S. Stoyanov, Y. Zhang, G. Hadjipanayis, D. Givord and J. Nogués, *Nature*, 2003, **423**, 850–853.

8 N. Arsalan, E. H. Kashi, A. Hasan, M. E. Doost, B. Rasti, B. A. Paray, M. Z. Nakhjiri, S. Sari, M. Sharifi, K. Shahpasand, K. Akhtari, S. Haghighat and M. Falahati, *Int. J. Nanomed.*, 2020, **15**, 4607–4623.

9 I. K. Kgosiemang, R. Lefojane, P. Direko, Z. Madlanga, S. Mashele and M. Sekhoacha, *Inorg. Nano-Met. Chem.*, 2020, **50**, 1070–1080.

This journal is © the Owner Societies 2023

Phys. Chem. Chem. Phys., 2023, **25**, 171–182 | 181

10 *Magnetic Nanoparticles: A New Platform for Drug Delivery*, ed. K. S. Joshy, T. Sabu and V. K. Thakur, Springer Nature Singapore Pte Ltd., 2021.

11 T. Morisato, N. Jones, S. Khanna and Y. Kawazoe, *Comput. Mater. Sci.*, 2006, **35**, 366–370.

12 F. Baletto and R. Ferrando, *Rev. Mod. Phys.*, 2005, **77**, 371–423.

13 P. Jena and A. W. Castleman, Jr., *Proc. Natl. Acad. Sci. U. S. A.*, 2006, **103**, 10560–10569.

14 C. J. Dibble, S. T. Akin, S. Ard, C. P. Fowler and M. A. Duncan, *J. Phys. Chem. A*, 2012, **116**, 5398–5404.

15 N. T. Mai, S. T. Ngo, P. Lievens, E. Janssens and N. T. Tung, *J. Phys. Chem. A*, 2020, **124**, 7333–7339.

16 A. Pramann, K. Koyasu, A. Nakajima and K. Kaya, *J. Phys. Chem. A*, 2002, **106**, 4891–4896.

17 C. N. van Dijk, D. R. Roy, A. Fielicke, T. Rasing, A. C. Reber, S. N. Khanna and A. Kirilyuk, *Eur. Phys. J. D*, 2014, **68**, 357.

18 F. Jiao and H. Frei, *Angew. Chem., Int. Ed.*, 2009, **48**, 1841–1844.

19 Y. Xie, F. Dong, S. Heinbuch, J. J. Rocca and E. R. Bernstein, *Phys. Chem. Chem. Phys.*, 2010, **12**, 947–959.

20 R. H. Aguilera-del Toro, F. Aguilera-Granja, A. Vega and L. C. Balbás, *Phys. Chem. Chem. Phys.*, 2014, **16**, 21732–21741.

21 N. T. Tung, N. M. Tam, M. T. Nguyen, P. Lievens and E. Janssens, *J. Chem. Phys.*, 2014, **141**, 044311.

22 A. O. H. Zayed, M. N. Daud and S. M. Zain, *J. Alloys Compd.*, 2017, **695**, 2513–2518.

23 G. L. Gutsev, K. G. Belay, K. V. Bozhenko, L. G. Gutsev and B. R. Ramachandran, *Phys. Chem. Chem. Phys.*, 2016, **18**, 27858–27867.

24 L. Geng, M. Weng, C.-Q. Xu, H. Zhang, C. Cui, H. Wu, X. Chen, M. Hu, H. Lin, Z.-D. Sun, X. Wang, H.-S. Hu, J. Li, J. Zheng, Z. Luo, F. Pan and J. Yao, *Natl. Sci. Rev.*, 2021, **8**, nwaa201.

25 J. van der Tol, PhD thesis, KU Leuven, 2019.

26 J. van der Tol and E. Janssens, *Phys. Rev. A*, 2020, **102**, 022806.

27 F. Neese, F. Wennmohs, U. Becker and C. Riplinger, *J. Chem. Phys.*, 2020, **152**, 224108.

28 C. Adamo and V. Barone, *J. Chem. Phys.*, 1999, **110**, 6158–6170.

29 F. Weigend and R. Ahlrichs, *Phys. Chem. Chem. Phys.*, 2005, **7**, 3297–3305.

30 J. M. Bakker, J. Jalink, D. Dieleman and A. Kirilyuk, *J. Phys.: Condens. Matter*, 2018, **30**, 494003.

31 T. Lu and F. Chen, *J. Comput. Chem.*, 2012, **33**, 580–592.

32 E. D. Glendening, C. R. Landis and F. Weinhold, *J. Comput. Chem.*, 2019, **40**, 2234–2241.

33 *Quantum mechanics*, ed. B. H. Bransden and C. J. Joachain, Pearson Education Ltd, 2nd edn, 2000.

34 T. H. Boyer, *Am. J. Phys.*, 1988, **56**, 688–692.

35 U. Rohrmann and R. Schäfer, *Phys. Rev. Lett.*, 2013, **111**, 133401.

36 M. Gleditzsch, T. M. Fuchs and R. Schäfer, *J. Phys. Chem. A*, 2019, **123**, 1434–1444.

37 X. Xu, S. Yin, R. Moro and W. A. de Heer, *Phys. Rev. B: Condens. Matter Mater. Phys.*, 2008, **78**, 054430.

38 G. F. Bertsch and K. Yabana, *Phys. Rev. A: At., Mol., Opt. Phys.*, 1994, **49**, 1930–1932.

39 M. B. Knickelbein, *Phys. Rev. B: Condens. Matter Mater. Phys.*, 2004, **70**, 014424.

40 U. Rohrmann, S. Schäfer and R. Schäfer, *J. Phys. Chem. A*, 2009, **113**, 12115–12121.

41 N. A. Spaldin, *Magnetic materials*, Cambridge University Press, 2nd edn, 2013.

42 R. M. Moon, *Phys. Rev.*, 1964, **136**, A195–A202.

43 C. T. Chen, Y. U. Idzerda, H.-J. Lin, N. V. Smith, G. Meigs, E. Chaban, G. H. Ho, E. Pellegrin and F. Sette, *Phys. Rev. Lett.*, 1995, **75**, 152–155.

44 V. Zamudio-Bayer, K. Hirsch, A. Langenberg, A. awicki, A. Terasaki, B. von Issendorff and J. T. Lau, *J. Phys.: Condens. Matter*, 2018, **30**, 464002.

45 S. Peredkov, M. Neeb, W. Eberhardt, J. Meyer, M. Tombers, H. Kampschulte and G. Niedner-Schatteburg, *Phys. Rev. Lett.*, 2011, **107**, 233401.

46 I. M. L. Billas, A. Châtelain and W. A. de Heer, *Science*, 1994, **265**, 1682–1684.

47 P. Ferrari and S. Gómez-Coca, *Phys. Chem. Chem. Phys.*, 2022, **24**, 23128–23134.

48 M. B. Knickelbein, *J. Chem. Phys.*, 2006, **125**, 044308.

49 F. W. Payne, W. Jiang, J. W. Emmert, J. Deng and L. A. Bloomfield, *Phys. Rev. B: Condens. Matter Mater. Phys.*, 2007, **75**, 094431.

50 J. Jalink, PhD thesis, Radboud Universiteit Nijmegen, 2014.

51 X. Xu, S. Yin, R. Moro and W. A. de Heer, *Phys. Rev. Lett.*, 2005, **95**, 237209.

52 J. L. Rodríguez-López, F. Aguilera-Granja, K. Michaelian and A. Vega, *Phys. Rev. B: Condens. Matter Mater. Phys.*, 2003, **67**, 174413.

53 J. Guevara, F. Parisi, A. M. Llois and M. Weissmann, *Phys. Rev. B: Condens. Matter Mater. Phys.*, 1997, **55**, 13283–13287.

54 H. T. Pham, N. T. Cuong, N. M. Tam, V. D. Lam and N. T. Tung, *Chem. Phys. Lett.*, 2016, **643**, 77–83.